PCCP

Check for updates

Non-touching plasma–liquid interaction – where is aqueous nitric oxide generated?†

Helena Jablonowski, [ID] *[a] Ansgar Schmidt-Bleker,[b] Klaus-Dieter Weltmann,[b] Thomas von Woedtke[b] and Kristian Wende [ID] [a]

Nitric oxide is a relatively stable free radical and an important signal molecule in plants, animals, and humans with high relevance for biological processes involving inflammatory processes, *e.g.* wound healing or cancer. The molecule can be detected in the gas phase of non-thermal plasma jets making it a valuable tool for clinical intervention, but transport efficiency from the gas phase into the liquid phase or tissue remains to be clarified. To elucidate this fact, the nitric oxide concentration in buffered solutions is determined using electron paramagnetic resonance spectroscopy. The origin of the nitric oxide in the liquid could be excluded, therefore, potential precursors such as hydroxyl radicals, superoxide anions, atomic hydrogen and stable species (nitrite, nitrate and hydrogen peroxide) were detected and the potential formation pathway as well as ways of enhancing the production of nitric oxide by alteration of the feed gas and the surrounding gas composition during plasma treatment of the liquid have been pointed out.

Introduction

Nitrogen oxides N_xO_y are major constituents of cold atmospheric pressure discharge, with N_2O_5, NO_2, N_2O alongside with HNO_2 and HNO_3 being frequently observed in the gas phase.[1–4] In plasma treated aqueous liquids, nitrite and nitrate ions are easily observed. Interestingly, also the biologically highly relevant nitric oxide ($^\bullet$NO) can be found in the gas phase and plasma treated liquids, sparking the interest of both fundamental and applied research.[5] The molecule is a comparably stable radical and has a key position in diverse biological cascades like vascular and neuronal signal transduction, cell death, or host defense.[6–8] The primary targets of $^\bullet$NO are specific heme-iron receptors, the soluble or bound guanylate cyclases (GCs), promoting the production of cyclic guanosine monophosphate as the major downstream effector.[9] Clinically, blood and tissue $^\bullet$NO levels are relevant for blood pressure regulation, platelet aggregation, control of inflammatory processes, and malignant diseases.[10,11] Nitric oxide is a double-edged sword, showing biphasic behaviour, *e.g.* in oncology; low concentrations undesirably promote tumor cell growth while higher concentration above 200 nM mediate tumor cell apoptosis.[12,13]

Contributing to this are oxidation processes of $^\bullet$NO which lead to the formation of N_2O_3 or nitrogen dioxide ($^\bullet$NO$_2$) and the reaction with superoxide anion radicals ($O_2^{\bullet-}$) forming the strong oxidant peroxynitrite ($ONOO^-$).[14] In contrast, topical application of $^\bullet$NO from chemical sources typically show beneficial effects in wound models.[15,16] Application of nitric oxide, especially topically, is challenging, *e.g.* due to the poor stability of $^\bullet$NO donor compounds or the intricate handling of gaseous $^\bullet$NO limiting clinical success. In this regard, cold physical plasma is a modern option to deliver $^\bullet$NO in a temporal and spatially controllable manner, rendering it interesting for therapeutic applications, *e.g.* in non-healing chronic wounds. Previous work has indicated the contribution of plasma derived nitrogen species, especially nitric oxide, on experimentally or clinically observed effects.[17–19] Further studies showed improved wound healing by cold plasma without specifying the active players but where the role of nitric oxide is discussed.[20–22]

Such an understanding of the deposition and/or generation processes of nitric oxide is key. As the solubility of $^\bullet$NO in water is rather low ($H^{cp}(^\bullet NO) = 1.9 \times 10^{-5}$ M Pa^{-1}), and gas phase densities are low to moderate, a mere gas phase generation of $^\bullet$NO and its subsequent solvation must be challenged.[23] In opposition, nitric oxide may be generated *via* chemical reactions between plasma generated reactive nitrogen and oxygen species in the bulk liquid or at the gas–liquid interface. Knowledge of the importance of the latter is growing and several recent publications emphasize its role over that of the bulk liquid.[24–29] However, as discussed by Bruggeman *et al.*, transport processes, chemical reactions in the bulk gas, the liquid

^{a} ZIK Plasmatis at Leibniz Institute for Plasma Science and Technology (INP Greifswald e.V.), Felix-Hausdorff-Str. 2, 17489 Greifswald, Germany. E-mail: helena.jablonowski@inp-greifswald.de

^{b} Leibniz Institute for Plasma Science and Technology (INP Greifswald e.V.), Felix-Hausdorff-Str. 2, 17489 Greifswald, Germany

This journal is © the Owner Societies 2018

Phys. Chem. Chem. Phys., 2018, **20**, 25387–25398 | 25387

phase, and at the interface occur simultaneously.[30] This makes the segregation of processes challenging, especially with the leak in gas–liquid interface diagnostic approaches. In many systems, the contribution of gas and liquid flow mechanics further escalates complexity ultimately driving research to focus on simulation approaches. Chen *et al.* modelled the oxygen-based chemistry of a surface helium–oxygen plasma by dividing it into a gas bulk model, a penetration model combined with Henry's law and a reaction chemistry part with the Poisson equation representing the gas–liquid interface, and for the bulk liquid a penetration model with reaction chemistry and the Poisson equation.[31] Verlackt *et al.* modelled the situation for a plasma jet similar to the one used in the presented study.[27] In their model, they could not find $^{\bullet}$NO in the bulk liquid, only in the interfacial region. Furthermore, their model predicts that long-lived species are mainly generated in the interface either by direct solvation or by reaction of, for instance, $^{\bullet}$NO originated from the gas phase.[27]

Here, the mechanism of nitric oxide deposition in physiological liquids by an argon plasma jet (kINPen09) was investigated. *Via* controlling of the ambient conditions and the working gas composition the possibility to regulate its $^{\bullet}$NO production was tested. Using electron paramagnetic resonance spectroscopy, ion chromatography, and colorimetric assays in combinations with gaseous $^{\bullet}$NO as control, a solvation of plasma derived $^{\bullet}$NO was excluded in favour of its *de novo* formation in the liquid. Furthermore, several potential gas or liquid phase precursors were ruled out and potentially dominating formation pathways were hypothesised.

Experimental

Plasma treatment

The plasma treatment took place in a 24 well plate using the well-characterized kINPen09 (neoplas GmbH, Greifswald, Germany) – a prior version of the certified medical product, the kINPen$^{\circledR}$ MED (neoplas tools GmbH, Greifswald, Germany) as the plasma source.[32–37] The plasma jet was equipped with a gas curtain device to enable working in a controlled environment.[38–41] The total feed gas flow of the kINPen09 was 3 standard litre per minute (slm), using argon (argon N50, Air Liquide, Paris, France) as feed gas with addition of 1% molecular gases, oxygen, and/or nitrogen (oxygen N48, nitrogen N50, Air Liquide, Paris, France). For some experiments, humidification of the feed gas was used; therefore, 1% of the feed gas was guided through a bubbler system (final humidity approximately 300 ppm). In the following, this experimental situation will be referred to as 'humidified feed gas', whereas the situation without explicit humidification of the feed gas will be referred to as 'dry feed gas'. The curtain gas device was fed with N_2 or synthetic air (nitrogen N50, synthetic air: 20.5 $\pm$ 0.5% O_2 in N_2, Air Liquide, Paris, France). A total curtain gas flow rate of 5 slm was used (see Fig. 1). Details about the effect of the curtain gas can be found in previous publications.[1,4,39,40]

In a 24 well plate, 750 μL of phosphate buffer (Na_2HPO_4/ H_2NaPO_4, Sigma Aldrich; 100 mM, pH 7.3) was treated for 30 s.
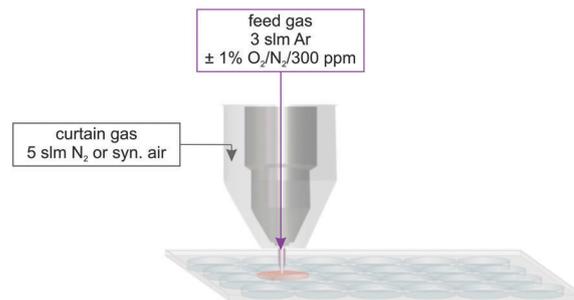

Fig. 1 Scheme for the plasma treatment of 750 μL phosphate buffer in a 24 well plate using the kINPen09 with an additional curtain gas device.

The distance between the plasma jet nozzle and the liquid surface was kept at 9 mm.[1] Furthermore, argon gas with 40 ppm $^{\bullet}$NO admixture was guided through the kINPen without igniting the plasma as a positive control.

Each data point consists of at least three independent samples; each sample was performed in triplicate. The error bars represent the minimal and maximal deviation of the mean value.

EPR measurements

For the detection of the $^{\bullet}$NO, $^{\bullet}$OH, $O_2^{\bullet-}$, and $^{\bullet}$H, electron paramagnetic resonance (EPR) spectroscopy was performed. An X-band (9.87 GHz) spectrometer (EMXmicro, Bruker BioSpin GmbH, Rheinstetten, Germany) was used with the following instrument parameters for all measurements: modulation frequency of 100 kHz, modulation amplitude of 0.1 mT, microwave power of 5.024 mW, receiver gain of 30 dB, and time constant of 0.01 ms. Depending on the used spin trap, the magnetic field scan was adjusted. A nitronyl nitroxyl radical (NNR) spin trap, carboxy-PTIO (2-(4-carboxyphenyl)-4,4,5,5-tetramethylimidazoline-1-oxyl-3-oxide, sodium salt), with an initial concentration of 60 μM, was used to detect $^{\bullet}$NO, giving an imino nitroxyl radical (INR) as a spin trap adduct with $^{\bullet}$NO,[42] whereas 10 mM BMPO (5-*tert*-butoxycarbonyl-5-methyl-1-pyrroline-*N*-oxide) was used for the detection of superoxide anion radicals ($O_2^{\bullet-}$) as well as hydroxyl radicals ($^{\bullet}$OH) and hydrogen radicals ($^{\bullet}$H). Due to economic reasons only selected data points (0, 0.2, 0.5, 0.8, 1% O_2 in Ar, 100% Ar, untreated and gas ctrl.) were measured using BMPO as a spin trap. Both spin traps were supplied from Dojindo Laboratoire (Kumamoto, Japan). For all EPR measurements, the spin trap was added to the phosphate buffer prior to plasma treatment to ensure trapping of all plasma generated radicals in the solution.

Prior to plasma treatment, an untreated spin trap solution (spin trap dissolved in phosphate buffer) was measured. Briefly, 50 μL of the treated or control solution was transferred to a borosilicate glass tube (125 mm length, 0.8525 mm inner diameter), and measured with a fixed delay of three minutes. EPR spectra evaluation was performed by using Bruker's Xenon software (Bruker BioSpin, Rheinstetten, Germany). Using the spin counting functionality and by calibrating the spectrometer, the absolute spin number could be determined. More details about the EPR procedure can be found in a previous publication.[43]

25388 | *Phys. Chem. Chem. Phys.*, 2018, **20**, 25387–25398

This journal is © the Owner Societies 2018

Ion chromatography

The detection of nitrite (NO_2^-) and nitrate (NO_3^-) was performed *via* ion chromatography (ICS-5000, Dionex Corp., Sunnyvale, USA). The ion chromatography measurements of nitrate and nitrite were performed as well only for the selected data points (0, 0.2, 0.5, 0.8, 1% O_2 in Ar, 100% Ar, untreated and gas ctrl.), which were investigated using BMPO as a spin trap for the EPR measurements. After treatment, the sample was diluted three fold using ultrapure water (MilliQ, Milli-Q® Merck KGaA, Darmstadt, Germany) before injecting 10 μL onto an IonPac® AS23 anion exchange column (2 × 250 mm, Thermo Fisher Scientific Inc., Waltham, USA). An isocratic mobile phase (4.5 mM Na_2CO_3/0.8 mM $NaHCO_3$) with 250 μL min^{-1} flow rate was used. Besides the use of the conductivity detector, data were collected as well from a UV detector (210 nm). The system was calibrated using the Dionex 7-anion standard on a weekly basis.

Colorimetric assay

Hydrogen peroxide (H_2O_2) was detected *via* a colorimetric reaction with xylenol orange using a commercially available assay (Pierce™ Quantitative Peroxide Assay Kit, Thermo Scientific, Rockford, USA) according to the manufacturer's protocol. The assay is based on the oxidation of ferrous to ferric ion by hydrogen peroxide in the presence of the dye which can be detected photometrically (Tecan Infinite M200 Pro, Tecan Group Ltd, Männedorf, Switzerland) at 595 nm. Each 96 well plate contained a set of standards for calibration (0 to 150 μM, in triplicates) and the samples ($n = 4$, in triplicate).

Results & discussion

In the following, possible reaction mechanisms that can lead to the generation of $^\bullet NO$ in systems are discussed. In the first paragraph below, the solvation of gaseous $^\bullet NO$ in the liquid is analysed since it is known from the literature[5,44] that the investigated plasma source produced $^\bullet NO$ in the gas phase. This process could be excluded as the predominant process for the origin of the liquid phase $^\bullet NO$. Therefore, in the following paragraph the focus is on the formation pathways yielding liquid phase $^\bullet NO$. Starting with a brief review regarding the relevant mechanisms that occur in the gas phase *via* the interfacial region, the bulk region, furthermore, multi-phase reactions and destruction reactions of $^\bullet NO$ are discussed.

Solvation of gaseous $^\bullet NO$

A previous study by Schmidt-Bleker *et al.* has shown that the generation of NO_x in the gas phase by the kINPen operated with an O_2/N_2 feed gas admixture can be enhanced by humidifying the feed gas.[5] That study has also shown that $^\bullet NO$ can also be detected in the far field (12 mm or more in front of the nozzle[5]) of the jet, if the feed gas is humidified and a N_2 gas curtain is applied. However, it is noted that in the near field (from the nozzle until 12 mm[1]) gaseous $^\bullet NO$ can be expected under all conditions to be present to some extent if at least some N_2 and O_2 or H_2O is available. As gaseous $^\bullet NO$ can quickly be oxidised
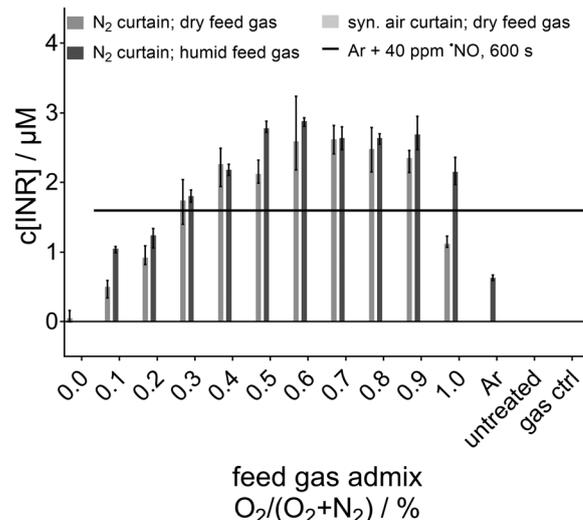

Fig. 2 $^\bullet NO$ spin adduct (INR) concentrations in the 30 s plasma treated phosphate buffer solution for different gas conditions compared to the $^\bullet NO$-concentration solvated during 600 s treatment with an Ar + $^\bullet NO$ gas mixture (40 ppm $^\bullet NO$ in Ar) as a function of the N_2 and O_2 content in the feed gas.

by various species (including $^\bullet O$, O_3, $HO_2^\bullet$, $^\bullet OH$; section '$^\bullet NO$ formation' reaction (6) and (7)), the detected downstream nitrogen oxides (H_xNO_y) are an indicator of the presence of $^\bullet NO$ in the effluent. To investigate the possible solvation of $^\bullet NO$ in the buffer solution, argon gas with 40 ppm $^\bullet NO$ admixture guided through the kINPen without igniting the plasma was used as a control. The results of the control compared to the plasma-generated concentration of the $^\bullet NO$ spin adduct (INR) in the liquid are shown in Fig. 2. For highlighting the difference obtained for $^\bullet NO$ concentration caused by plasma treatment and by just guiding an Ar + $^\bullet NO$ gas stream onto the liquid, in Fig. 2 already the plasma generated $^\bullet NO$-adduct concentration is given. Details about the plasma treatment data are given in the following sections. Remarkably, to reach a similar INR concentration in the phosphate buffer solution, the pure gas treatment time had to be extended to 600 s, which was 20-fold of the plasma treatment time. Furthermore, the used $^\bullet NO$-density of 40 ppm was more than fivefold higher than the estimated amount generated by the kINPen in the gas phase, which is calculated to be less than 8 ppm at maximum according to the following assumption. In order to estimate the maximum possible $^\bullet NO$ density in the gas phase, all nitrogen oxides measured *via* FTIR spectroscopy in the gas phase reported in Schmidt-Bleker *et al.* are added: these include besides $^\bullet NO$, also $^\bullet NO_2$, HNO_2, HNO_3 and N_2O_5 which are all likely downstream products of $^\bullet NO$.[5] From the literature, a density of up to 8 ppm in the maximum of the gaseous phase $^\bullet NO$ can be estimated and by assuming a linear increase of $^\bullet NO$ transfer (due to Henry's law) to the liquid from the gas phase[4,5] (which is subsequently trapped by the spin trap) in an ideal case, 16 nM INR could originate from solvation of gaseous $^\bullet NO$ following a 30 s treatment with the kINPen, which is well below the measured concentrations.

Hence, a pure solvation process of gaseous $^\bullet$NO can be excluded, and it can be stated that the determined $^\bullet$NO in the buffer solution had its origin in the liquid or at the gas/liquid interface region. The aqueous equilibrium concentration of a species at a given partial gas pressure is described by the Henry coefficient. $^\bullet$NO ($H^{cp}(^\bullet NO) = 1.9 \times 10^{-5}$ M Pa^{-1}) is only moderately soluble in water.[23,45] Since the solubility of $^\bullet$NO$_2$ is also low, (although tenfold higher than the solubility of $^\bullet$NO); ($H^{cp}(^\bullet NO_2) = 1.2 \times 10^{-4}$ M Pa^{-1}), solvation of gaseous $^\bullet$NO$_2$ is also an unlikely source for the $^\bullet$NO detected in plasma-treated liquid, even if all dissolved $^\bullet$NO$_2$ was converted to $^\bullet$NO.[46] It is mentioned that the solubility of both HNO$_2$ and HNO$_3$ is higher by several orders of magnitude ($H^{cp}(HNO_2) = 4.8 \times 10^{-1}$ M Pa^{-1}, $H^{cp}(HNO_3) = 2.1 \times 10^{3}$ M Pa^{-1}),[46] which are present in the gas phase at densities of up to 1 ppm according to a study of Schmidt-Bleker et al.[5]

Since the detected liquid phase $^\bullet$NO was not mainly generated in the gas phase and transferred into the liquid, other formation pathways have to be taken into account. Possible generation pathways of aqueous $^\bullet$NO are discussed in the following.

$^\bullet$NO formation

By the use of electron paramagnetic resonance spectroscopy and the nitronyl nitroxyl radical (NNR) as a spin trap, the $^\bullet$NO adduct, imino nitroxyl radical (INR), was determined. This determined concentration of the $^\bullet$NO adduct (INR) is given in Fig. 3, whereby in Fig. 3a the concentration for humidified feed gas and in Fig. 3b for dry feed gas is shown as a function of the O$_2$ content in the feed gas. The feed gas composition was not always argon with 1% admixture (varied from 1% N$_2$ and 0% O$_2$ to 0% N$_2$ and 1% O$_2$) also pure argon (Ar) was used. With increasing O$_2$ content in the feed gas the INR concentration was raised until a maximal concentration of almost 3 μM for both humidified and dry feed gas. This maximal concentration was reached for an intermediate amount of O$_2$ in the feed gas before it decreased again. The controls, untreated buffer solution and gas treated (only feed gas without plasma ignition) yielded no INR signals. Ar treatment instead resulted in a formation of INR, whereby it differed for humid and dry feed gas. Only with humidity added to the feed gas is the concentration detectable. In addition, the maximum in INR formation was at different intermediate O$_2$ contents in the feed gas depending on whether humid or dry feed gas was applied. For the dry condition, the maximum was shifted more to a higher O$_2$ content (0.6% to 0.8% O$_2$) whereas for humidified feed gas it was around 0.5% to 0.6% O$_2$. The shift is only minor and by taking the error bars into account the maximum was for the humid and for the dry feed gas condition in the range between 0.5 or 0.4 to 0.9% O$_2$, respectively. In the humid condition, there was also one plasma treatment condition where no INR was determined, more specifically, for a feed gas composition of 1% N$_2$ and 99% Ar. This was not the case for dry conditions, although the INR concentration for that feed gas admixture was by far the lowest detected. Even though there were differences observed for humid and dry feed gas, these
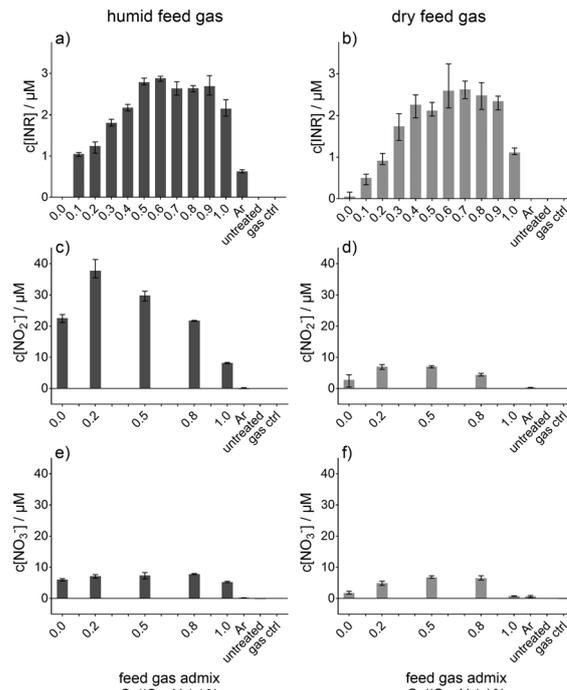

Fig. 3 Concentration of nitric oxide spin trap adduct (a) and (b), nitrite (c) and (d), and nitrate (e) and (f). Each column represented either humid (left column) or dry (right column) feed gas for a N$_2$ curtain gas. The concentrations were obtained after 30 s plasma treatment of phosphate buffer and given as function of the O$_2$ content (%) in the feed gas argon (Ar). "Ar" indicates treatment with pure argon without the O$_2$/N$_2$ admixture; "gas ctrl" indicates treatment with pure gas mixture without plasma ignition; "untreated" indicates pure phosphate buffer without any treatment.

were not so remarkable that it could be stated that one of these two condition yielded a surplus in INR, and therefore, $^\bullet$NO-formation. In contrast, the observed dynamic of the INR concentration due to the feed gas admixtures of O$_2$ and N$_2$ have an important impact onto the $^\bullet$NO-formation. Besides the $^\bullet$NO formation via INR, the formed concentrations of NO$_2^-$ (Fig. 3c and d) and NO$_3^-$ (Fig. 3e and f) are given as well as a function of the O$_2$ content in the humidified (Fig. 3c and e) or dry feed gas (Fig. 3d and f). Other than INR, NO$_2^-$ showed a remarkably different behaviour between the humid and dry feed gas; with humidified feed gas, the resultant concentrations were several fold higher than for dry feed gas. Furthermore, the maximal yielded NO$_2^-$ concentration was found for 0.2% O$_2$ and 0.8% N$_2$ in the feed gas for both the humid and dry feed gas condition. NO$_3^-$ did not alter much, although it was slightly more produced for 0%, 0.2%, and 1% O$_2$ in the humid feed gas than in the dry condition.

Beside these nitrogen species also some potentially relevant oxygen species, O$_2^{\bullet-}$, $^\bullet$OH, and H$_2$O$_2$ as well as atomic hydrogen ($^\bullet$H) were investigated under the same conditions (see Fig. 4). The radical adducts of O$_2^{\bullet-}$ (Fig. 4a and b), $^\bullet$OH (Fig. 4c and d), and $^\bullet$H (Fig. 4e and f) were determined by EPR using BMPO as a spin trap. The concentration of H$_2$O$_2$ is given in Fig. 4g and h. The behaviour of O$_2^{\bullet-}$ (BMPO-$^\bullet$OOH, Fig. 4a and b) showed only slight differences for humid or dry feed gas. Under the humid
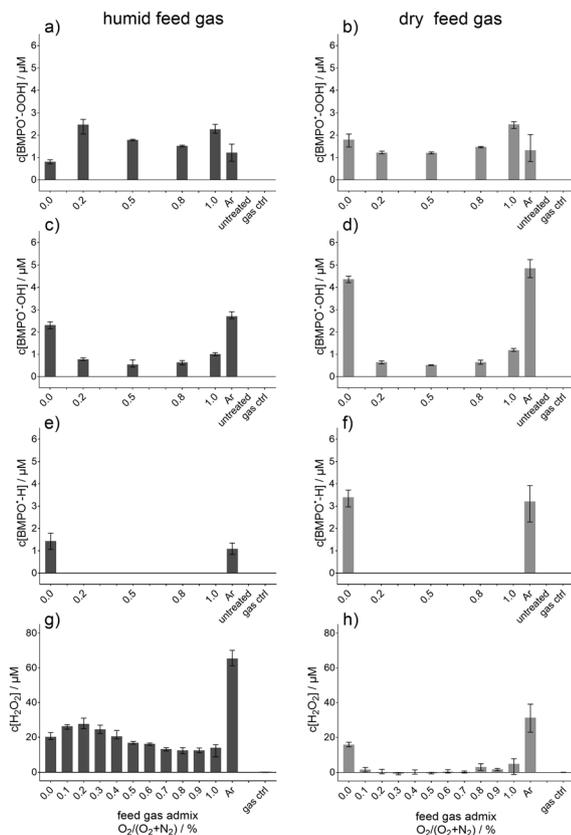
25390 | Phys. Chem. Chem. Phys., 2018, **20**, 25387–25398

This journal is © the Owner Societies 2018

Fig. 4 Concentration of $O_2^{\bullet-}$ spin trap adduct (a) and (b), $^{\bullet}OH$ spin trap adduct (c) and (d), $^{\bullet}H$ spin trap adduct (e) and (f), and H_2O_2 (g) and (h). Each column represented either humid (left column) or dry (right column) feed gas for a N_2 curtain gas. The concentrations were obtained after 30 s plasma treatment of phosphate buffer and given as a function of the O_2 content (%) in the feed gas argon (Ar). ''Ar'' indicates treatment with pure argon without O_2/N_2 admixture; ''gas ctrl'' indicates treatment with pure gas mixture without plasma ignition; ''untreated'' indicates pure phosphate buffer without any treatment.

condition, an O_2 content of 0.2% yielded the highest concentration, whereas the maximum was reached for dry feed gas for 1% followed by the 0% O_2 admixture. For 0% O_2 content in the humid feed gas instead, the lowest BMPO$^{\bullet}$-OOH concentration was determined. The difference between the humid and dry feed gas was clearer for the $^{\bullet}OH$ (BMPO$^{\bullet}$-OH, Fig. 4c and d). There, the O_2 free conditions, pure Ar and Ar + 1% N_2 as dry feed gas, resulted in almost twice as high concentrations as for the humid feed gas. The other feed gas compositions did not vary between humid and dry. The difference between humid and dry was also observed for the same two pronounced feed gas compositions for $^{\bullet}H$ (BMPO$^{\bullet}$-H, Fig. 4e and f). Under the O_2 containing feed gas conditions no BMPO$^{\bullet}$-H was detected. A strong relation of the H_2O_2 concentration to humid feed gas was observed (Fig. 4g), whereby pure Ar yielded the maximum. For dry feed gas (Fig. 4h), pure Ar resulted as well in the highest concentration, although it was less than half of the one of the humid feed gas. A further difference was observed for Ar + 1% N_2, a condition which resulted in higher H_2O_2 concentration than all other dry feed gas compositions, whose concentrations were much lower.

In the following, other potential formation pathways than solvation are discussed and weighted in consideration of the above described measurement results.

Although the $^{\bullet}NO$ in the liquid phase was not predominantly generated in the gas phase and solvated in the liquid, at least some of the precursors of the liquid phase $^{\bullet}NO$ had their origin in the gaseous phase. Hence, in the following subsection a more detailed insight into the formation of several precursors in the gas and plasma phase is briefly reviewed. Following the gaseous phase reactions, the gas–liquid interface and the bulk liquid reaction involved in either precursor or direct $^{\bullet}NO$ formation are discussed. Furthermore, in the subsection 'multi-phase reactions' reactions which occur in more than one of the discussed phases are taken into account for the formation of $^{\bullet}NO$ in the liquid or at its interface.

Nitrogen oxides generated in gas phase processes. The generation of aqueous $^{\bullet}NO$ requires that at some point the strong N_2-triple bond (bond energy of 9.79 eV) is broken. This process is likely to occur in the plasma, where excited species with high energies (e.g. excited Ar-species with energies of 11.5 eV and more) are available and lead to direct dissociation of N_2 via the reaction (1).

$$Ar^* + N_2 \rightarrow 2N + Ar^1 \tag{1}$$

N_2 can also be excited through electron impact, e.g. forming metastable nitrogen $N_2(A)$ which carries 6.2 eV (ESI,† reaction (S1)).

A numerical study of the kINPen operated with O_2/N_2 feed gas admixtures suggests that gaseous $^{\bullet}NO$ is mainly formed through the reaction (2).

$$N_2^* + {^{\bullet}O} \rightarrow {^{\bullet}NO} + N^{47} \tag{2}$$
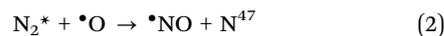
Also the extended Zeldovich mechanism, which comprises the reactions (3)–(5) can remarkably contribute to the generation of gaseous $^{\bullet}NO$.[48]

$$N_2 + {^{\bullet}O} \rightarrow {^{\bullet}NO} + N \tag{3}$$

$$O_2 + N \rightarrow {^{\bullet}NO} + {^{\bullet}O} \tag{4}$$

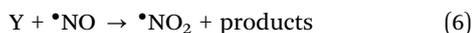$$N + {^{\bullet}OH} \rightarrow {^{\bullet}NO} + {^{\bullet}H} \tag{5}$$

Note that the original mechanisms proposed by Zeldovich (reactions (3) and (4)) require elevated temperatures (typically 1000 K and more) to occur. Solely, the latter reaction (5) can occur at room temperature, and hence, may be the only one of high relevance in situations where plasma is brought into close contact with water. It yields $^{\bullet}OH$ and $^{\bullet}H$ from dissociation of water molecules (ESI,† reaction (S2)), where X* denotes an excited species (such as N_2^*, Ar^*, or $O(1D)$) or electrons with sufficient energy to break the H–OH bond with a bond energy of 5.17 eV.[49]

The latter reaction (5) also implies that generation of N or N_2^* as a precursor for the generation of $^{\bullet}NO$ in the liquid (reactions (2)–(4)) is unlikely to occur in the liquid itself, since reactive species with sufficient energy are most likely to dissociate water (ESI,† reaction (S2)). Hence, it is most likely that $^{\bullet}NO$ is either transferred from the gaseous to the liquid phase

(discussed in paragraph 'Solvation of gaseous $^\bullet$NO'), or generated though secondary reactions from further nitrogen oxides generated in the core plasma, or at the liquid interface. The dominant nitrogen oxides that can be expected in the effluent of the kINPen comprise $^\bullet$NO$_2$, which can be generated from $^\bullet$NO by various oxidizing agents Y (such as O$_3$, $^\bullet$O, HO$_2$$^\bullet$) in reactions of the form of reaction (6) and HNO$_2$ and HNO$_3$, which are mainly generated in reactions such as reaction (7).[47]

$$Y + {}^\bullet NO \rightarrow {}^\bullet NO_2 + products \qquad (6)$$

$$^\bullet NO_x + {}^\bullet OH \rightarrow HNO_{x+1} \qquad (7)$$

Interface reactions. The solution was buffered yielding a pH of 7.3. While this solution does have a large bulk buffer capacity, it is unclear if it is sufficient to maintain a neutral pH at the surface of the liquid. According to the measurements by Schmidt-Bleker *et al.*, HNO$_2$ and HNO$_3$ densities in the order of 1 ppm can be expected in the gas phase.[5] Applying Henry's law locally at the liquid surface suggests that 1 ppm of HNO$_3$ in the gas phase would be sufficient to create 350 mM HNO$_3$ and 60 μM HNO$_2$ in the liquid phase. While the actual concentration at the liquid surface can hardly be determined, it is noted that a local concentration of 175 mM HNO$_3$ is already sufficient to achieve a pH value of 3.0 (calculated numerically using aqion Pro, written by H. Kalka[50]). At such pH levels, further reactions can take place that may contribute to the generation of $^\bullet$NO, for instance, the generation of $^\bullet$NO from nitrous acid, the protonated form of NO$_2$$^-$, which proceeds *via* formation of N$_2$O$_3$ (ESI,† reaction (S3)) and reaction (8).[51]
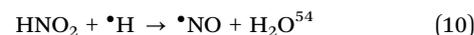
$$N_2O_3 \leftrightarrow {}^\bullet NO_2 + {}^\bullet NO \qquad (8)$$

Due to the low pK_a = 3.4 of HNO$_2$, the formation of N$_2$O$_3$ (ESI,† reaction (S3)) is more likely to occur at low pH. However, numerical simulation suggests that during plasma treatment the H$_3$O$^+$ concentration may indeed be several orders of magnitude higher in the interfacial region compared to that of the bulk liquid.[52] Therefore, these reactions could only take place in the interface.

Another mechanism that is well-known in the context of plasma-treated liquids is the generation of peroxynitrous acid (ONOOH) in the reaction (9) whereas ONOOH partially (3 to 30%) decomposes to form $^\bullet$NO$_2$ and $^\bullet$OH, where ONOOH could act as precursors for the generation of $^\bullet$OH.[53]

$$HNO_2 + H_2O_2 \rightarrow ONOOH + H_2O \rightarrow {}^\bullet NO_2 + {}^\bullet OH + H_2O \qquad (9)$$
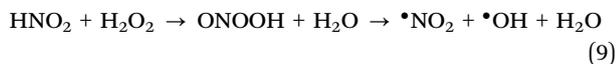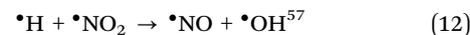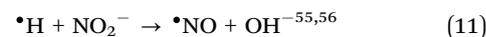
The reaction (9) preferably occurs at low pH values. Lukes *et al.* formulated the rate coefficient as the reaction between the sum of HNO$_2$ and NO$_2$$^-$ as the pH-dependent rate.[53] For instance, at pH 3 the rate coefficient for this reaction is 4 M^{-1} s^{-1}, which is too low to have a remarkable impact on the generation of the potential $^\bullet$NO precursor $^\bullet$NO$_2$. In particular this is the case, since a maximum of only 30% of the formed ONOOH decomposed to $^\bullet$NO$_2$. Hence, even if the relevant amounts of H$_2$O$_2$ are present in the liquid, and therefore, available for ONOOH/ONOO$^-$ formation, this pathway could not be the dominant one.

Reaction (10) could also occur at the surface of the liquid, where the pH is low enough for relevant amounts of HNO$_2$ to exist.
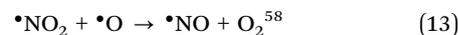
$$HNO_2 + {}^\bullet H \rightarrow {}^\bullet NO + H_2O^{54} \qquad (10)$$

The rate coefficient is also reasonably high (4.5 × 10^8 M^{-1} s^{-1}), thus reaction (10) could contribute to the generation of $^\bullet$NO in the liquid. Assuming HNO$_2$ originated from the gas phase and $^\bullet$H from the liquid, as was measured for two conditions in the bulk liquid (see Fig. 4e and f), the presence of $^\bullet$H required the absence of O$_2$ in the curtain gas. Moreover, the absence of O$_2$ in the feed gas was necessary as well to detect $^\bullet$H in the bulk liquid. As shown in Fig. 4e and f, BMPO$^\bullet$-H was only determined for pure Ar feed gas and Ar + 1% N$_2$. Ar + 1% N$_2$ was, according to Schmidt-Bleker *et al.*, not suitable for the formation of gas phase HNO$_2$.[5] This led to the conclusion that reaction (10) could not be one of the dominant formation reactions of liquid phase $^\bullet$NO.

Bulk reactions. Also in the bulk liquid, $^\bullet$H can lead to the generation of $^\bullet$NO *via* the fast (k_{17} = 7.1 × 10^8 M^{-1} s^{-1}) reaction (11) or *via* reaction (12), a reaction well known also from gaseous systems (k_{18} = 1.47 × 10^{-10} cm^{-3} s^{-1}).

$$^\bullet H + NO_2^- \rightarrow {}^\bullet NO + OH^{-55,56} \qquad (11)$$

$$^\bullet H + {}^\bullet NO_2 \rightarrow {}^\bullet NO + {}^\bullet OH^{57} \qquad (12)$$

While these reactions may contribute to the generation of aqueous $^\bullet$NO, they are not likely to be the predominant mechanism leading to the generation of aqueous $^\bullet$NO in the current set of experiments. By comparison of the measured trends for the $^\bullet$NO adduct (see Fig. 3a and b) with the ones of the potential precursors, NO$_2$$^-$ (see Fig. 3c and d) and $^\bullet$H (see Fig. 4e and f), it becomes obvious that the trends do not fit each other. As mentioned during the discussion of reaction (10), BMPO$^\bullet$-H was only detectable for pure Ar feed gas and Ar + 1% N$_2$ no matter whether the feed gas was humidified or dry. The $^\bullet$NO adduct (INR) was instead not observable for dry Ar feed gas as well as for humid Ar + 1% N$_2$ feed gas. This is the first hint that the reaction is probably not the predominant pathway. In addition, by taking a closer look into the NO$_2$$^-$ trends, also here, the observed concentrations are not suitable; pure Ar feed gas yielded only traces of NO$_2$$^-$ in the bulk liquid under dry and humid conditions. Moreover, during treatment with humid Ar + 1% N$_2$ feed gas, NO$_2$$^-$ as well as $^\bullet$H were formed but no $^\bullet$NO adduct was produced. These contrasts together with the fact that the concentration of the $^\bullet$NO adduct was independent of humid or dry feed gas but the precursors assumed from reaction (11) were dependent on the humidity are contradictory. Hence, reaction (11) could be excluded as the dominant pathway.

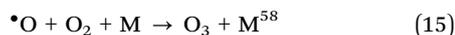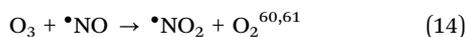A relevant mechanism could be the generation of $^\bullet$NO from $^\bullet$NO$_2$ through reaction (13).

$$^\bullet NO_2 + {}^\bullet O \rightarrow {}^\bullet NO + O_2^{58} \qquad (13)$$

While no rate coefficients were found for this reaction in liquids, the corresponding gas phase rate coefficient is

25392 | *Phys. Chem. Chem. Phys.*, 2018, **20**, 25387–25398

This journal is © the Owner Societies 2018

$k_{19} = 1.03 \times 10^{-11}$ cm^3 s^{-1}, implying that this process could be relevant in liquids as well.[58] If reaction (13) is a main source of aqueous $^\bullet$NO, the question arises as to how $^\bullet$NO$_2$ is generated in or transferred to liquids. Some reactions which can lead to the generation of $^\bullet$NO$_2$ in the interface have already been discussed under 'Interface Reactions' such as the decomposition of HNO$_2$ via N$_2$O$_3$ (reaction (8) and reaction (S3), ESI†) or the decay of the ONOOH (reaction (9)). Furthermore, also a formation in the gas phase such as the mentioned reaction (6) could be origin of that $^\bullet$NO precursor.

The promoting effect of a N$_2$ curtain gas could have a double impact; on one hand the N$_2$ could be an additional source of the N-containing precursors as was discussed during the prior processes. On the other hand, it avoids the formation of huge amounts of gaseous O$_3$ which inhibits the formation of aqueous $^\bullet$NO by destroying precursors necessary for its generation.[59] For instance, NO$_2^-$ could effectively be removed from the liquid via O$_3$ (ESI† reaction (S4)).

O$_3$ is a double-edged sword as well; it can also contribute to the formation of $^\bullet$NO$_2$ via reaction with the gas phase $^\bullet$NO (reaction (14)). Although the optimum for O$_3$ production was not under N$_2$ curtain gas, there will be still a relevant amount produced in the gas phase with an N$_2$ curtain, especially for higher admixtures of O$_2$.[5] There, also the three body reaction of $^\bullet$O with O$_2$ and a third body (M) takes place (reaction (15)).

$$O_3 + {}^\bullet NO \rightarrow {}^\bullet NO_2 + O_2 \quad^{60,61} \qquad (14)$$

$$^\bullet O + O_2 + M \rightarrow O_3 + M \quad^{58} \qquad (15)$$

However, as mentioned above, an $^\bullet$O-related process leading to an increase of $^\bullet$NO production is more likely than an O$_3$-related process preventing $^\bullet$NO-production. The reason is that the $^\bullet$NO density continuously rises from 0 to 0.6% O$_2$ content in the feed gas (see Fig. 3a and b), while both $^\bullet$O and O$_3$ can be expected to increase with additional O$_2$ content in the feed gas.

At first sight, an $^\bullet$O-related process cannot explain the measured INR density in the case using the N$_2$ curtain with the 1% N$_2$ feed gas admixture and dry feed gas (Fig. 3b), where no $^\bullet$O can be expected. There, the only way to create $^\bullet$O in the liquid under this condition is the complete dissociation of H$_2$O into $^\bullet$H and $^\bullet$OH in the first step and in the second step $^\bullet$OH into $^\bullet$O and $^\bullet$H. With a bond dissociation energy of 5.17 eV (first step) and 4.44 eV (second step), this is in principle possible under these conditions.[35] For dry feed gas, the dissociation took place in the gas phase, whereas for the N$_2$ curtain with the 1% N$_2$ feed gas admixture, the process occurred in the interface. In the literature, the generation via a reaction of NO$_2^-$ with $^\bullet$H has been mentioned in an aqueous system (see reaction (11)).[55]
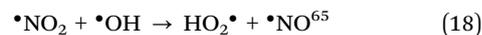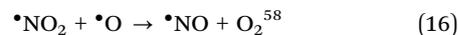
$^\bullet$H has recently been measured in the effluent of an Ar-operated plasma operated with an Ar gas curtain jet.[62] Additionally, $^\bullet$H can be generated from solvated electrons e$^-$ via the reaction with H$^+$ (see ESI,† reaction (S5)).

However, this process is unlikely in these experiments, since the effluent of the plasma jet does not directly touch the liquid surface.

In Fig. 3c–f, the generated concentrations of NO$_2^-$ and NO$_3^-$ after plasma treatment are given over the O$_2$ feed gas admixture, whereby, the concentrations given in Fig. 3c and e represented the humid and Fig. 3d and f the dry feed gas.

Interestingly, there was a strong difference between these two; humidification of the feed gas yielded a much more pronounced formation of NO$_2^-$ compared to NO$_3^-$. NO$_3^-$ was detected in similar amounts for the humid and dry feed gas. In the latter case, also the NO$_2^-$ was in the same concentration range, up to 8 μM. The difference in these two cases suggests that a NO$_2^-$-related mechanism may not be the predominant pathway of the liquid phase $^\bullet$NO formation because the trend and amounts of $^\bullet$NO formation are similar in the humid and dry feed gas (see Fig. 3a and b). The observed trends for NO$_2^-$, NO$_3^-$ and $^\bullet$NO for dry feed gas are similar. In contrast, the trends for humid feed gas are not alike. Hence, in that case, the detected NO$_2^-$ and NO$_3^-$ is predominantly produced via a different pathway than via $^\bullet$NO for the humid and dry feed gas condition; for instance, the solvation of gaseous HNO$_2$ and HNO$_3$ could be highly relevant.

Multi-phase reactions. In a plasma system, several other reactions could contribute to the formation as well as there are many reactive species present simultaneously. For instance, some reactions known from the gas phase could occur in the interface or the liquid as well. These reactions usually include oxygen species, for instance, $^\bullet$O, O$_3$, or $^\bullet$OH (reaction (2) and reactions (16)–(21)). As the solvation processes could be excluded as the predominant pathway for the $^\bullet$NO in the liquid and it was found that there was a difference in NO$_2^-$ generation between dry and humid feed gas, further pathways most likely contribute to the formation of $^\bullet$NO in the liquid. For instance, reactions containing other nitrogen centred radicals and/or oxygen radicals such as in reactions (12), (13), (14), (16)–(20).

$$^\bullet NO_2 + {}^\bullet O \rightarrow {}^\bullet NO + O_2 \quad^{58} \qquad (16)$$

$$^\bullet N + {}^\bullet OH \rightarrow {}^\bullet NO + H^\bullet \quad^{63,64} \qquad (17)$$

$$^\bullet NO_2 + {}^\bullet OH \rightarrow HO_2{}^\bullet + {}^\bullet NO \quad^{65} \qquad (18)$$

$$^\bullet NO_2 + {}^\bullet N \rightarrow 2{}^\bullet NO \quad^{66} \qquad (19)$$

$$^\bullet N + {}^\bullet O \rightarrow {}^\bullet NO \quad^{67} \qquad (20)$$

In general, another possible formation reaction of $^\bullet$NO would be the reaction of $^\bullet$O with $^\bullet$N, which could be formed by plasma as well (reaction (20)).[67] The precursors had to be generated at least partially in the gas phase. To evaluate the reaction probability of nitrogen containing precursors with $^\bullet$H, $^\bullet$OH, or O$_2^{\bullet-}$, these three species were analysed by the use of spin trap enhanced EPR spectroscopy.

The concentration of the generated spin trap adduct for O$_2^{\bullet-}$/HO$_2^\bullet$, $^\bullet$OH, and $^\bullet$H was determined using BMPO as a spin trapping agent as it is able to distinguish between the O$_2^{\bullet-}$- and $^\bullet$OH-adduct.[43,68]

In Fig. 4, the resulting concentrations for the trapped O$_2^{\bullet-}$ (a), $^\bullet$OH (c), and $^\bullet$H (e) are shown in the case of humidified feed gas admixtures and N$_2$ as the curtain gas. Interestingly, under plasma treatment conditions (with O$_2$ in the feed gas), where

higher amounts of •NO were detected (see Fig. 3a), the concentration of •OH was lower (see Fig. 4c). In contrast, high •OH-adduct concentrations were observed – pure Ar or Ar + 1% N_2 as feed gas – for conditions where no or just minor amounts of •NO were measured after plasma treatment. Without the admixture of O_2, the •OH-adduct concentration was maximal (see Fig. 4c and d). Moreover, when O_2 was present in the humidified feed gas, the BMPO•-OH concentration was reduced by 50% or more. This dependence on the feed gas humidity indicated no direct linkage of the •OH with the formation of •NO. It could be also excluded that •OH is consumed by the formation of •NO, as there were treatment conditions where different concentrations of the •OH adduct were detected, for instance the N_2 curtain gas with 0.2% or 0.8% O_2 admixture to the feed gas. Here, the determined concentrations of the •NO spin probe adduct differed a lot whereas those of the •OH adduct were similar. A similar situation was observable for humidified feed gas for the 0.2% and 1% O_2 feed gas admixture.

For •H, the observations were almost the same, besides that in the case of O_2 present in the humid feed gas no BMPO•-H adduct was detectable, presumably because gaseous •H quickly reacts with O_2, leading to the generation of HO_2• (ESI,† reaction (S6)).

This would also imply that solvation from the gas phase is the predominant source of •H detected in the liquid or at least the formation in the bulk liquid or at the interface was hindered by presence of O_2 in the feed gas. Furthermore, •H can also quite likely be generated at the liquid surface by dissociation of water; under O_2-free conditions VUV radiation can reach the liquid surface as mentioned above.[35] For the kINPen09, the argon excimer radiation at 126 nm is present and is able to dissociate H_2O.[35]

As already discussed when considering the NO_2^--formation, also •H does probably not predominantly contribute to the production of •NO via reaction (11).

The O_2•−-adduct behaved slightly differently; the lowest BMPO•-OOH concentrations reached for these humidified plasma treatments were observed when only N_2 was added to the feed gas. When N_2 was used as the curtain gas, no diffusion of O_2 from the environment took place. Hence, the results for O_2•− were as expected when the O_2•− mainly originated from the gas phase. There, HO_2• will be generated and can be transferred to the liquid.[1,5] In general, the production of O_2•− adducts in all other conditions, Ar and Ar with O_2 addition, was more pronounced when the feed gas was humidified. Due to the pH value of 7.3 of the used phosphate buffer, the HO_2• will be present in its deprotonated form as O_2•−.[45] The highest concentration was detected for the 0.2% and 1% O_2 admixture in the humid feed gas. The reason for the maximum at the 1% O_2 admixture could be the simultaneous formation of •OH and O_3 in the gas phase. If both species react with each other, HO_2• could be formed (see ESI,† reaction (S7)). For 0.2% O_2 in the feed gas, one reaction, which enhanced the O_2•−/HO_2• formation could be •O with H_2O_2 (see ESI,† reaction (S8)), as by addition of humidity to the feed gas the formation of H_2O_2 will

be enhanced.[33,69] This was also shown here under these specific conditions. This will be discussed in more detail later on.

For dry feed gas and N_2 curtain gas, the BMPO-adducts of O_2•−, •OH, and •H are given in Fig. 4b, d and f. For O_2-free conditions, the measured concentrations for BMPO•-OH and BMPO•-H were about twice the one of the humidified feed gas plasma treatment. This indicated again that also the formation of •NO via •OH and •H was not likely to be the predominant process.

In contrast, the feed gas humidity did not influence the O_2•− adduct concentration as much as the •OH adduct concentration; the O_2•− adduct concentrations were in the same range for both dry and humid feed gas. Interestingly, for the dry feed gas, the two highest conditions were obtained for the 1% O_2 and 1% N_2 feed gas. In particular the admixture of only N_2 was in contrast to the humidified case, as there the lowest BMPO•-OOH concentration was observed. Due to the absence of O_2 in the gas phase, the high energetic species could reach the interfacial region and the liquid surface yielding reduction of the liquid phase O_2 to O_2•−. In the case of the 1% O_2 admixture, the HO_2• could also be mainly produced in the plasma/gas phase as was the case for humidified feed gas, although, direct production in the liquid itself was likely as well. For instance, reactions of •OH, •O, O_3, and H_2O_2 (see ESI,† reactions (S7)–(S10)) could result in an increase of O_2•−/HO_2• in the solution.

The fact that humidity yields no surplus for the formation of oxygen radicals in liquids is known from the literature, although, in that study only humidity but no O_2 and N_2 was added.[69]

As mentioned above, the H_2O_2 concentration in strongly linked to the feed gas humidity. Concentrations in Fig. 4g were detected after plasma treatment with humidified feed gas. The highest concentration, more than threefold higher than that of the others, was obtained for pure Ar. Interestingly, low amounts of O_2, up to 0.2% yielded slightly higher H_2O_2 concentrations than those for only N_2 or N_2 with 0.3% O_2 or more for humidified feed gas. For BMPO-OOH a similar increase was observed for the humidified feed gas and it is known from the literature that HO_2•/O_2•− could contribute to the formation of H_2O_2 as well.[31,45] This explained this slight increase. The other conditions all resulted in almost the same concentration, although the oxygen radical concentrations inside the liquid differed. This underlined the predominant formation of H_2O_2 in the gas phase if humidity was added to the feed gas.[69]

In contrast to the humidified feed gas, the dry feed gas yielded much lower H_2O_2 concentrations for all cases of feed gas admixtures of N_2 and/or O_2 (Fig. 4h). Between the 0.1% and 0.7% O_2 admixture the determined concentrations were in the range of the lower detection limit of the assay used, which was 1 μM according to the data sheet of the manufacturer. For higher amounts of O_2, there was a slight increase observed, but not in the range of what was measured for the 1% N_2 admixture or for pure argon. Under these two conditions (pure Ar or Ar + 1% N_2), high energetic radiation or species such as V(UV) and metastable nitrogen were able to reach the liquid

25394 | *Phys. Chem. Chem. Phys.*, 2018, **20**, 25387–25398

This journal is © the Owner Societies 2018

and dissociate water to $^\bullet$OH (see subsection 'Bulk reactions'), yielding *via* recombination H_2O_2.[35,44,70]

Looking at all results together, it can be stated that it was most likely that the aqueous $^\bullet$NO production was linked to reactions containing $^\bullet$N/$NO_2^\bullet$ and $^\bullet$O/O_3.

Destruction and regulation of $^\bullet$NO production. Although the oxygen radicals were evaluated regarding their contribution in the generation of $^\bullet$NO in the liquid, they are able to destruct it as well (see ESI,† reactions (S7) and (S8)). Furthermore, possible destruction reactions could occur also *via* reactions of $^\bullet$NO with $^\bullet$H (ESI,† reaction (S9)). Moreover, also O_3, O_2, or other nitrogen species can be involved in the destruction of $^\bullet$NO (reactions (21)–(29)). In the long-term view, without spin trapping agents or other organic molecules present in the solution, $^\bullet$NO will result in NO_2^- and finally in NO_3^-.

$$^\bullet NO + O_2^{\bullet -} \rightarrow ONOO^{-64} \tag{21}$$

$$^\bullet NO + {}^\bullet OH \rightarrow NO_2^- + H^{+71} \tag{22}$$

$$^\bullet NO + {}^\bullet H \rightarrow HNO^{72} \tag{23}$$

$$^\bullet NO + O_3 \rightarrow {}^\bullet NO_2 + O_2^{73} \tag{24}$$

$$4^\bullet NO + O_2 + 2H_2O \rightarrow 4H^+ + 4NO_2^- \tag{25}$$

$$2^\bullet NO + O_2 \rightarrow 2^\bullet NO_2^{74} \tag{26}$$

$$^\bullet NO_3 + {}^\bullet NO \rightarrow 2^\bullet NO_2^{58} \tag{27}$$

$$^\bullet NO_2 + {}^\bullet NO \rightarrow N_2O_3^{75} \tag{28}$$

$$N_2O_3 + 2OH^- \rightarrow 2NO_2^- + H_2O^{75} \tag{29}$$

As relevant amounts of BMPO-OOH have also been detected in the liquid (see Fig. 3a and b), it was likely that some $^\bullet$NO is removed by $O_2^{\bullet -}$ or $HO_2^\bullet$ in reactions (21) and (30).

$$HO_2^\bullet + {}^\bullet NO \rightarrow ONOOH^{76} \tag{30}$$
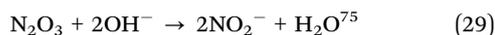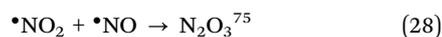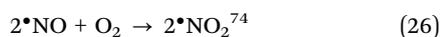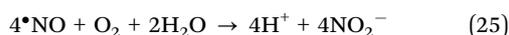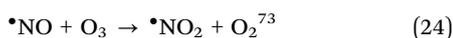
While up to 30% of the generated ONOOH could be regenerated to $^\bullet NO_2$[53] and subsequently $^\bullet$NO *via* various pathways, $HO_2^\bullet$ still is expected to lead to a net reduction of the $^\bullet$NO content in the liquid. If not stabilized by a spin trap, $HO_2^\bullet$ is also likely to quickly vanish by reaction with $^\bullet$OH (ESI,† reaction (S11)) or with another $HO_2^\bullet$ molecule (ESI,† reaction (S12)).

In the previous study concerning the reactive species output of the kINPen in the gas phase, NO_x were produced in similar amounts either with N_2 curtain gas or with the synthetic air curtain.[5] However, in the present study, the synthetic air environment around the plasma plume completely inhibits the formation of aqueous $^\bullet$NO (no INR was detected in this case; data not shown, the corresponding NNR signal is shown in Fig. 5).

Based on the mechanisms discussed in the literature, it is assumed that the exclusion of ambient O_2 will mainly have two effects: first, when ambient O_2 is excluded (while O_2 is still admixed to the feed gas), $^\bullet$O is more likely and O_3 less likely to reach the liquid surface, as less $^\bullet$O is converted to O_3 in the gas phase by reaction (15).[1,5]
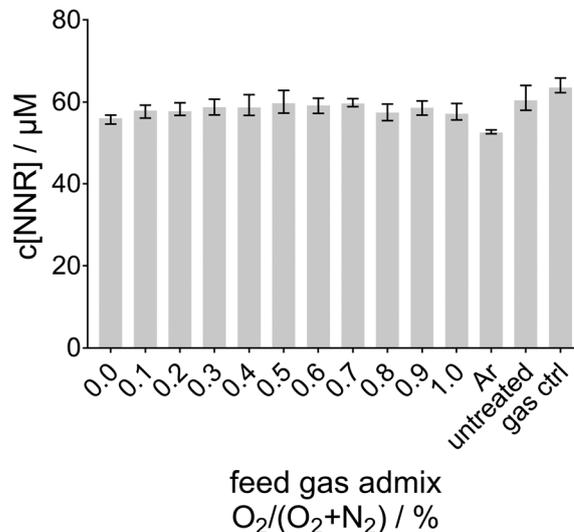
Fig. 5 The nitronyl nitroxyl radical concentration for a synthetic air curtain gas and dry molecular feed gas admixtures obtained after 30 s plasma treatment as a function of the O_2 content in the feed gas.

In a prior study, among others, the effect of the curtain gas on the oxygen species production was investigated.[77] There, also the suppression of the $^\bullet$O concentration in the liquid in the presence of synthetic air surroundings was determined. In that study, increasing amounts of O_2 up to 1%, but no N_2, were added to the feed gas. By the use of TEMPD-HCl as a spin probe $^\bullet$O, $^1O_2$, or O_3 were detected after plasma treatment. Due to the gaseous formation processes, it could be stated that for direct treatment, as was the case in the here-presented study as well, the N_2 curtain gas mainly leads to the formation of aqueous $^\bullet$O, whereas an extended treatment distance or a synthetic air curtain gas composition was dominated by the formation of O_3.[77] This leads to the conclusion that $^\bullet$O is an important precursor for aqueous $^\bullet$NO, and in the presence of O_2, O_3 is formed, which prevents the formation of aqueous $^\bullet$NO. Therefore, using synthetic air as the curtain gas, it was expected that less or no $^\bullet$NO-adducts are detectable in the plasma treated phosphate buffer. In contrast to the measurements using N_2 curtain gas using either humid (see Fig. 3a) or dry feed gas (see Fig. 3b), for synthetic air as the curtain gas no INR was detected. In Fig. 5, the nitronyl nitroxyl radical (NNR) concentration is plotted as no INR was detected after plasma treatment. This was the expected result, as due to the presence of O_2 in the surroundings mainly O_3 is formed. Interestingly, the spin trap concentration from initially 60 µM was slightly reduced due to the plasma treatment. This destruction of the compound was most prominent in the case of pure argon as feed gas. Under this condition, only diffusing species from the surroundings into the plasma plume were excited, therefore, more highly energetic argon species reached the liquid and effected the spin trap therein. Besides the highly energetic argon species, also other radicals present in the liquid such as $^\bullet$OH, $^\bullet$O, and $O_2^{\bullet -}$ could react with the spin trap compound yielding non-paramagnetic products. This point is discussed in more detail

This journal is © the Owner Societies 2018

Phys. Chem. Chem. Phys., 2018, 20, 25387–25398 | 25395
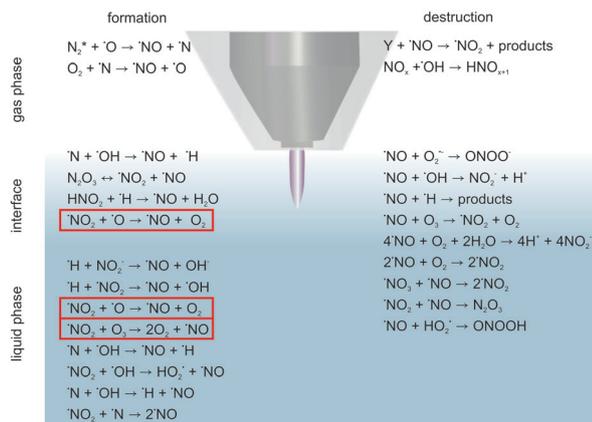
Scheme 1 A detailed look into the relevant formation and destruction reactions of $^\bullet$NO in the gas phase, interface, and the liquid phase. Red frames indicate the most likely formation reactions for liquid phase $^\bullet$NO.

in the paragraph '$^\bullet$NO formation'. Second, $^\bullet$H can be expected to reach the liquid surface when ambient O_2 is excluded, which quickly forms $HO_2^\bullet$ by reaction with a third body (M) in the reaction (S6) (ESI†). As the rate for the gas phase reaction (S6) (ESI†) is fast $(5.65 \times 10^{-32} \text{ cm}^6 \text{ s}^{-1})$, already small amounts of O_2 from feed gas admixtures inhibit the transport of gaseous $^\bullet$H to the liquid surface. As shown in Fig. 4e and f, $^\bullet$H was only detected in the liquid if no O_2 is available in the ambient or the feed gas. More details about the role of $^\bullet$H in the formation processes of $^\bullet$NO can be found in the subsection 'Bulk reactions'.

Conclusions

In the present study, the origin of $^\bullet$NO was investigated. It was known from previous studies that different reactive species induced by the plasma jet have various origins. Here, it could be shown for the first time that liquid phase $^\bullet$NO mainly originated from the bulk and interfacial region and not *via* solvation from the gas phase. This knowledge is of high importance for the impact of plasma treatment on targets, no matter whether they are biological targets or not. Increasing knowledge about the ongoing chemical reactions are essential for matching the treatment condition and the aimed application.

The predominant formation and destruction reactions are given in Scheme 1, where the most relevant reactions occurring in the different phases – gas phase, interface, and liquid phase – are put together. By combination of the measurements with knowledge about the gas phase chemistry of the plasma jet from the literature and theoretical considerations of possible formation reactions, the most likely reactions for $^\bullet$NO production were determined: this pointed to the liquid in the direction of reactions of nitrogen species with $^\bullet$O/O_3, which are highlighted by red frames in Scheme 1. The elucidation of the relevant formation reaction added to the overall understanding of the induced chemistry by the kINPen09. Besides this, the elucidated optimum for the formation of $^\bullet$NO by kINPen09 enables a regulation of the $^\bullet$NO formation as desired in the

application, for instance, for tailored therapeutic treatment in cancer medicine or wound healing.

Conflicts of interest

There are no conflicts to declare.

Acknowledgements

References

1 A. Schmidt-Bleker, J. Winter, A. Bösel, S. Reuter and K.-D. Weltmann, *Plasma Sources Sci. Technol.*, 2015, **25**, 015005.

2 T. Moiseev, N. Misra, S. Patil, P. Cullen, P. Bourke, K. Keener and J. Mosnier, *Plasma Sources Sci. Technol.*, 2014, **23**, 065033.

3 S. Iseni, S. Reuter and K. D. Weltmann, *J. Phys. D: Appl. Phys.*, 2014, **47**, 075203.

4 A. V. Pipa, S. Reuter, R. Foest and K. D. Weltmann, *J. Phys. D: Appl. Phys.*, 2012, **45**, 085201.

5 A. Schmidt-Bleker, R. Bansemer, S. Reuter and K.-D. Weltmann, *Plasma Process Polym.*, 2016, **13**, 1120–1127.

6 O. I. Aruoma, *J. Am. Oil Chem. Soc.*, 1998, **75**, 199–212.

7 A. J. Gow and H. Ischiropoulos, *J. Cell. Physiol.*, 2001, **187**, 277–282.

8 J. R. Hickok, D. Vasudevan, K. Jablonski and D. D. Thomas, *Redox Biol.*, 2013, **1**, 203–209.

9 D. A. Fitzpatrick, D. M. O'Halloran and A. M. Burnell, *BMC Evol. Biol.*, 2006, **6**, 26.

10 Y. C. Luiking and N. E. Deutz, *Curr. Opin. Clin. Nutr. Metab. Care*, 2003, **6**, 103–108.

11 P. Pacher, J. S. Beckman and L. Liaudet, *Physiol. Rev.*, 2007, **87**, 315–424.

12 S. Huerta, *Future Sci. OA*, 2015, **1**, FSO44.

13 W. Xu, L. Z. Liu, M. Loizidou, M. Ahmed and I. G. Charles, *Cell Res.*, 2002, **12**, 311–320.

14 K. Kobayashi, M. Miki and S. Tagawa, *J. Chem. Soc., Dalton Trans.*, 1995, 2885–2889.

15 L. R. Martinez, G. Han, M. Chacko, M. R. Mihu, M. Jacobson, P. Gialanella, A. J. Friedman, J. D. Nosanchuk and J. M. Friedman, *J. Invest. Dermatol.*, 2009, **129**, 2463–2469.

16 M. Neidrauer, U. K. Ercan, A. Bhattacharyya, J. Samuels, J. Sedlak, R. Trikha, K. A. Barbee, M. S. Weingarten and S. G. Joshi, *J. Med. Microbiol.*, 2014, **63**, 203–209.

17 C. V. Suschek and C. Opländer, *Clinical Plasma Medicine*, 2016, **4**, 1–8.

18 A. B. Shekhter, V. A. Serezhenkov, T. G. Rudenko, A. V. Pekshev and A. F. Vanin, *Nitric oxide*, 2005, **12**, 210–219.

19 V. N. Vasilets, A. B. Shekhter, A. E. Guller and A. V. Pekshev, *Clinical Plasma Medicine*, 2015, **3**, 32–39.

25396 | *Phys. Chem. Chem. Phys.*, 2018, **20**, 25387–25398

This journal is © the Owner Societies 2018

20 G. Isbary, J. L. Zimmermann, T. Shimizu, Y. F. Li, G. E. Morfill, H. M. Thomas, B. Steffes, J. Heinlin, S. Karrer and W. Stolz, *Clinical Plasma Medicine*, 2013, **1**, 19–23.

21 G. Isbary, J. L. Zimmermann, T. Shimizu, G. E. Morfill, A. Mitra, H. Thomas, T. G. Kaempfl, J. Koeritzer, V. Boxhammer, J. Schlegel and W. Stolz, *Plasma Medicine*, 2012, **2**, 85–96.

22 A. Schmidt, S. Bekeschus, K. Wende, B. Vollmar and T. von Woedtke, *Exp. Dermatol.*, 2017, **26**, 156–162.

23 R. Sander, *Atmos. Chem. Phys.*, 2015, **15**, 4399–4981.

24 A. D. Lindsay, D. B. Graves and S. C. Shannon, *J. Phys. D: Appl. Phys.*, 2016, **49**, 235204.

25 K. Wende, P. Williams, J. Dalluge, W. V. Gaens, H. Aboubakr, J. Bischof, T. von Woedtke, S. M. Goyal, K. D. Weltmann, A. Bogaerts, K. Masur and P. J. Bruggeman, *Biointerphases*, 2015, **10**, 029518.

26 C. E. Anderson, N. R. Cha, A. D. Lindsay, D. S. Clark and D. B. Graves, *Plasma Chem. Plasma Process.*, 2016, **36**, 1393–1415.

27 C. C. W. Verlackt, W. Van Boxem and A. Bogaerts, *Phys. Chem. Chem. Phys.*, 2018, **20**, 6845–6859.

28 N. Kurake, H. Tanaka, K. Ishikawa, K. Takeda, H. Hashizume, K. Nakamura, H. Kajiyama, T. Kondo, F. Kikkawa, M. Mizuno and M. Hori, *J. Phys. D: Appl. Phys.*, 2017, **50**, 155202.

29 Y. Y. Zhao, T. Wang, M. P. Wilson, S. J. MacGregor, I. V. Timoshkin and Q. C. Ren, *IEEE Trans. Plasma Sci.*, 2016, **44**, 2084–2091.

30 P. J. Bruggeman, M. J. Kushner, B. R. Locke, J. G. E. Gardeniers, W. G. Graham, D. B. Graves, R. C. H. M. Hofman-Caris, D. Maric, J. P. Reid, E. Ceriani, D. F. Rivas, J. E. Foster, S. C. Garrick, Y. Gorbanev, S. Hamaguchi, F. Iza, H. Jablonowski, E. Klimova, J. Kolb, F. Krcma, P. Lukes, Z. Machala, I. Marinov, D. Mariotti, S. M. Thagard, D. Minakata, E. C. Neyts, J. Pawlat, Z. L. Petrovic, R. Pflieger, S. Reuter, D. C. Schram, S. Schroter, M. Shiraiwa, B. Tarabova, P. A. Tsai, J. R. R. Verlet, T. von Woedtke, K. R. Wilson, K. Yasui and G. Zvereva, *Plasma Sources Sci. Technol.*, 2016, **25**, 053002.

31 C. Chen, D. X. Liu, Z. C. Liu, A. J. Yang, H. L. Chen, G. Shama and M. G. Kong, *Plasma Chem. Plasma Process.*, 2014, **34**, 403–441.

32 S. Reuter, J. Winter, S. Iseni, S. Peters, A. Schmidt-Bleker, M. Dunnbier, J. Schafer, R. Foest and K. D. Weltmann, *Plasma Sources Sci. Technol.*, 2012, **21**, 034015.

33 J. Winter, K. Wende, K. Masur, S. Iseni, M. Dunnbier, M. U. Hammer, H. Tresp, K. D. Weltmann and S. Reuter, *J. Phys. D: Appl. Phys.*, 2013, **46**, 295401.

34 A. Schmidt-Bleker, S. A. Norberg, J. Winter, E. Johnsen, S. Reuter, K. D. Weltmann and M. J. Kushner, *Plasma Sources Sci. Technol.*, 2015, **24**, 035022.

35 H. Jablonowski, R. Bussiahn, M. U. Hammer, K. D. Weltmann, T. von Woedtke and S. Reuter, *Phys. Plasmas*, 2015, **22**, 122008.

36 S. Bekeschus, A. Schmidt, K.-D. Weltmann and T. von Woedtke, *Clinical Plasma Medicine*, 2016, **4**, 19–28.

37 K. D. Weltmann, E. Kindel, R. Brandenburg, C. Meyer, R. Bussiahn, C. Wilke and T. von Woedtke, *Contrib. Plasma Phys.*, 2009, **49**, 631–640.

38 S. Reuter, J. Winter, A. Schmidt-Bleker, H. Tresp, M. U. Hammer and K. D. Weltmann, *IEEE Trans. Plasma Sci.*, 2012, **40**, 2788–2794.

39 S. Reuter, H. Tresp, K. Wende, M. U. Hammer, J. Winter, K. Masur, A. Schmidt-Bleker and K. D. Weltmann, *IEEE Trans. Plasma Sci.*, 2012, **40**, 2986–2993.

40 H. Tresp, M. U. Hammer, K.-D. Weltmann and S. Reuter, *Plasma Medicine*, 2013, **3**, 45–55.

41 H. Jablonowski, M. A. Haensch, M. Duennbier, K. Wende, M. U. Hammer, K. D. Weltmann, S. Reuter and T. von Woedtke, *Biointerphases*, 2015, **10**, 029506.

42 N. Hogg, *Free Radical Biol. Med.*, 2010, **49**, 122–129.

43 H. Tresp, M. U. Hammer, J. Winter, K. D. Weltmann and S. Reuter, *J. Phys. D: Appl. Phys.*, 2013, **46**, 435401.

44 S. Iseni, P. J. Bruggeman, K.-D. Weltmann and S. Reuter, *Appl. Phys. Lett.*, 2016, **108**, 184101.

45 B. Halliwell and J. M. C. Gutteridge, *Free Radicals in Biology and Medicine*, Oxford University Press, Oxford, 2007.

46 R. Sander, *Atmos. Chem. Phys.*, 2015, **15**, 4399–4981.

47 W. V. Gaens, S. Iseni, A. Schmidt-Bleker, K. D. Weltmann, S. Reuter and A. Bogaerts, *New J. Phys.*, 2015, **17**, 033003.

48 J. Zeldovich, *Eur. Phys. J. A*, 1946, **21**, 577–628.

49 M. H. Stans, NIST Special Publication 1, 1970, p. 58.

50 H. Kalka, www.aqion.de http://www.aqion.de/.

51 E. Kaiser and C. Wu, *J. Phys. Chem.*, 1977, **81**, 1701–1706.

52 W. Tian, A. M. Lietz and M. J. Kushner, *Plasma Sources Sci. Technol.*, 2016, **25**, 055020.

53 P. Lukes, E. Dolezalova, I. Sisrova and M. Clupek, *Plasma Sources Sci. Technol.*, 2014, **23**, 015019.

54 C. C. Hsu, M. C. Lin, A. M. Mebel and C. F. Melius, *J. Phys. Chem. A*, 1997, **101**, 60–66.

55 B. Smaller, E. C. Avery and J. R. Remko, *J. Chem. Phys.*, 1971, **55**, 2414–2418.

56 W. Tian and M. J. Kushner, *J. Phys. D: Appl. Phys.*, 2014, **47**, 165201.

57 M. C. Su, S. S. Kumaran, K. P. Lim, J. V. Michael, A. F. Wagner, L. B. Harding and D. C. Fang, *J. Phys. Chem. A*, 2002, **106**, 8261–8270.

58 R. Atkinson, D. L. Baulch, R. A. Cox, J. N. Crowley, R. F. Hampson, R. G. Hynes, M. E. Jenkin, M. J. Rossi and J. Troe, *Atmos. Chem. Phys.*, 2004, **4**, 1461–1738.

59 Y. Gorbanev, N. Stehling, D. O'Connell and V. Chechik, *Plasma Sources Sci. Technol.*, 2016, **25**, 055017.

60 B. T. J. van Ham, S. Hofmann, R. Brandenburg and P. J. Bruggeman, *J. Phys. D: Appl. Phys.*, 2014, **47**, 224013.

61 F. Girard, M. Peret, N. Dumont, V. Badets, S. Blanc, K. Gazeli, C. Noel, T. Belmonte, L. Marlin, J. P. Cambus, G. Simon, N. Sojic, B. Held, S. Arbault and F. Clement, *Phys. Chem. Chem. Phys.*, 2018, **20**, 9198–9210.

62 S. Yatom, Y. C. Luo, Q. Xiong and P. J. Bruggeman, *J. Phys. D: Appl. Phys.*, 2017, **50**, 415204.

63 I. W. Smith and D. W. Stewart, *J. Chem. Soc., Faraday Trans.*, 1994, **90**, 3221–3227.

This journal is © the Owner Societies 2018

Phys. Chem. Chem. Phys., 2018, **20**, 25387–25398 | 25397

64 V. G. Kharitonov, A. R. Sundquist and V. S. Sharma, *J. Biol. Chem.*, 1994, **269**, 5881–5883.

65 D. Chakraborty, J. Park and M. Lin, *Chem. Phys.*, 1998, **231**, 39–49.

66 L. F. Phillips and H. I. Schiff, *J. Chem. Phys.*, 1965, **42**, 3171–3174.

67 K. Niemi, D. O'Connell, N. de Oliveira, D. Joyeux, L. Nahon, J. P. Booth and T. Gans, *Appl. Phys. Lett.*, 2013, **103**, 034102.

68 F. A. Villamena and J. L. Zweier, *J. Chem. Soc., Perkin Trans. 2*, 2002, 1340–1344, DOI: 10.1039/b201734b.

69 J. Winter, H. Tresp, M. U. Hammer, S. Iseni, S. Kupsch, A. Schmidt-Bleker, K. Wende, M. Dunnbier, K. Masur, K. D. Weltmannan and S. Reuter, *J. Phys. D: Appl. Phys.*, 2014, **47**, 285401.

70 S. Bekeschus, S. Iseni, S. Reuter, K. Masur and K. D. Weltmann, *IEEE Trans. Plasma Sci.*, 2015, **43**, 776–781.

71 W. A. Seddon, J. W. Fletcher and F. Sopchysh, *Can. J. Chem.*, 1973, **51**, 1123–1130.

72 R. Knight and H. Sutton, *Trans. Faraday Soc.*, 1967, **63**, 2628–2639.

73 J. Hoigne, H. Bader, W. R. Haag and J. Staehelin, *Water Res.*, 1985, **19**, 993–1004.

74 J. S. Beckman and W. H. Koppenol, *Am. J. Physiol.*, 1996, **271**, C1424–C1437.

75 M. Grätzel, S. Taniguchi and A. Henglein, *Ber. Bunsen-Ges.*, 1970, **74**, 488–492.

76 S. Goldstein and G. Czapski, *Free Radical Biol. Med.*, 1995, **19**, 505–510.

77 H. Jablonowski, J. S. Sousa, K.-D. Weltmann, K. Wende and S. Reuter, *Sci. Rep.*, 2018, **8**, 12195.

25398 | *Phys. Chem. Chem. Phys.*, 2018, **20**, 25387–25398

This journal is © the Owner Societies 2018